Please do not adjust margins

Journal Name

COMMUNICATION

Room Temperature-processed Inverted Organic Solar Cells using High Working-Pressure-Sputtered ZnO film

Received 00th January 20xx,
Accepted 00th January 20xx

DOI: 10.1039/x0xx00000x

www.rsc.org/

Il Jeon,[a] Yang Qian,[a] Shoichiro Nakao,[b] Daisuke Ogawa,[c] Rong Xiang,[a] Taiki Inoue,[a] Shohei Chiashi,[a] Tetsuya Hasegawa,[b,c] Shigeo Maruyama,[a] and Yutaka Matsuo[a,e]**

This study reports improved performance of inverted organic solar cells by using high working-pressure sputtered ZnO. Sputtering produces high crystalline ZnO without the need for thermal annealing. However, photovoltaic application of sputtered ZnO has shown lower power conversion efficiencies than those made by sol-gel ZnO. On the other hand, the sol-gel ZnO limits the flexible application of inverted organic solar cells because of high-temperature annealing. Therefore, a new method of sputtering under high working-pressure is developed. Power conversion efficiency of inverted organic solar cells fabricated using this high working-pressure-sputtered ZnO (η= 8.6%, V_{OC} = 0.77 V, J_{SC} = 15.6 mA cm^{-2}, FF = 0.72) supersedes that of the conventional sol-gel ZnO-based devices (η = 7.8%, V_{OC} = 0.73 V, J_{SC} = 16.0 mA cm^{-2}, FF = 0.63). Furthermore, utilizing low temperature process of sputtering, flexible application is successfully achieved using polyethylene terephthalate indium tin oxide film.

Organic solar cells (OSCs) have received much attention in recent years due to their potential as the next-generation of clean and efficient light harvesting devices.[1–3] Moreover, there are substantial benefits to be gained from the organic thin-film structure, which translates to flexible device application.[4–7] In inverted OSCs, ZnO plays a major role as an electron-transporting layer (ETL).[8–10] ZnO forms an ohmic contact with ITO and the active layer, because its conduction-band edge (−4.4 eV) is located between the conduction-band edge of ITO (−4.7 eV) and the LUMO energy level of electron acceptors (−3.8 eV).[8–10] ZnO is currently the best-performing electron transporting layer (ETL) among candidates such as TiO_x,[11] Cs_2CO_3, and Al_2O_3[12], due to its high mobility and reduced light-soaking effect. Currently, the most widely used method of depositing ZnO is the sol-gel method reported by Heeger and his colleagues.[13–17] However, it has been well known that high performance ZnO film requires high temperature thermal annealing, which limits the flexibility of application.[18-20] Low-temperature ZnO processes have been developed, but they render OSCs with low power conversion efficiencies (PCEs).[21–25] There are other techniques that undergo a low temperature ZnO fabrication, —namely plasma-enhanced chemical vapour deposition (PEC-VD),[26] microwaves plasma chemical vapour deposition (MPCVD),[27] atomic layer deposition (ALD),[28] and sputtering, the latter of which has attracted lately.[29] Sputtering not only operates at low temperature, but is also able to deposit dense, homogeneous, and reproducible ZnO films with well-defined c-axis orientation even when deposited on amorphous rigid substrates.[30] Researchers commonly think the solution process is cheaper than the sputtering method. However, sputtering is also compatible with the roll-to-roll process under high deposition rates which makes it low-cost process as well.[31,32] What is more, since the substrate, indium tin oxide (ITO) is sputtered anyway, its cost-issue can be resolved if ZnO is sputtered right after the ITO deposition.

Despite the numerous merits of the sputtering technique, high PCE has not been reported from sputtered ZnO-based OSCs to date.[30,33–35] Some report that high-temperature annealing on sputtered ZnO can improve PCEs, but it defies the objective of using sputter technique over solution process.[36] There is a two-step method that evades high-temperature annealing, but this technique is disadvantageous in terms of its ability to produce high-quality film with low V_{OC} and the number of steps.[33,37]

In this paper, we report high-performance a one-step ZnO film sputtering technique that utilizes high working-pressure (HWP). HWP reduced the energy of high-energy particles such as recoiled Ar and negatively charged oxygen, based on previous studies in TiO_2. This led to higher crystallinity and increased the conductivity of ZnO films, owing to reduced

[a] Department of Mechanical Engineering, School of Engineering, The University of Tokyo, 7-3-1 Hongo, Bunkyo-ku, Tokyo 113-8656, Japan
[b] Kanagawa Academy of Science and Technology 3-2-1 Sakado, Takatsu-ku, Kawasaki 213-0012, Japan
[c] Department of Chemistry, School of Science, The University of Tokyo, 7-3-1 Hongo, Bunkyo-ku, Tokyo 113-0033, Japan
[d] National Institute of Advanced Industrial Science and Technology (AIST), 1-2-1 Namiki, Tsukuba, Ibaraki 305-8564, Japan
[e] Hefei National Laboratory for Physical Sciences at the Microscale, University of Science and Technology of China, Hefei, Anhui 230026, China

Electronic Supplementary Information (ESI) available: [Sputtered ZnO working-pressure splits test, sputtered ZnO oxygen partial pressure splits test, sputtered ZnO thermal annealing test, sputtered ZnO optical analysis, and literature comparisons]. See DOI: 10.1039/x0xx00000x

This journal is © The Royal Society of Chemistry 20xx

Please do not adjust margins

Please do not adjust margins

recombination centers. The high quality of HWP-sputtered ZnO was proven by a strong c-axis (002) peak from X-ray diffraction spectroscopy (XRD) and O-Zn peak from X-ray photoelectron spectroscopy (XPS). On the basis of the finding, inverted OSCs were fabricated as shown in **Figure 1**. The devices demonstrated a PCE of 8.6% in thieno[3,4-b]thiophene/benzodithiophene (PTB7) and [6,6]-phenyl C71-butyric acid methyl ester ($PC_{71}BM$)-used inverted OSCs with an open-circuit voltage (V_{OC}) of 0.77 V and a fill factor (FF) of 0.72, while sol-gel ZnO-based device showed a PCE of 7.8% with a V_{OC} of 0.73 and a FF of 0.65. The increases in both the V_{OC} and FF denote the superior film-quality of the HWP-sputtered ZnO films. Furthermore, a flexible OSC was fabricated on an ITO / polyethylene terephthalate (PET) substrate and produced a PCE of 4.4%.

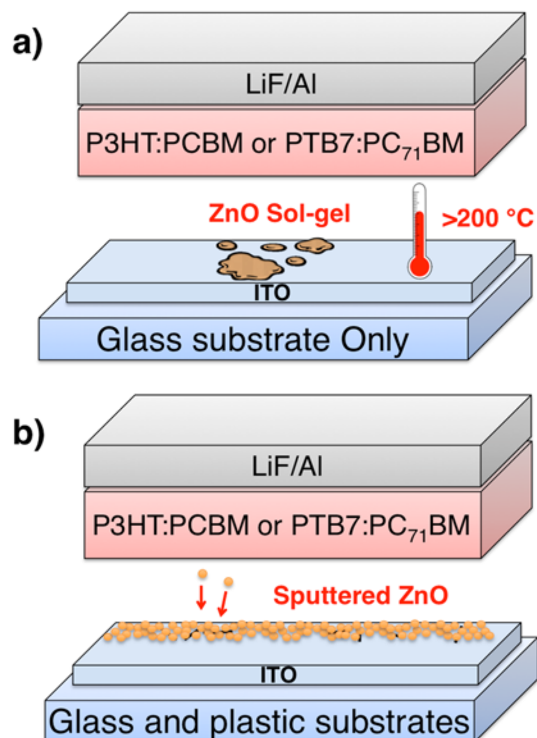

Fig. 1. Illustrations of (a) sol-gel ZnO-based inverted OSC and (b) sputtered ZnO-based inverted OSC.

The crystallinity of ZnO films was investigated using XRD (**Figure 2**). HWP-sputtered ZnO films showed a (002) peak at 34.26°, in addition to a (103) peak at 63.81°; on the other hand, the sol-gel ZnO films showed no peaks. This reveals that the sputter-grown ZnO films have a wurtzite structure (JCPDS card No 36-1451), while the sol-gel ZnO films have an amorphous layer with small crystallites size.[38] This also shows that HWP-sputtered ZnO possessed c-axis preferred growth. Such favourable effect can be attributed to the better control of the sputtered particles in a HWP atmosphere. In general, working-pressure is optimized to produce dense films with high crystallinity, which belong to zone T structure in the Thornton model.[39] Because the formation of zone T structure is assisted by the bombardment of high energy (100~1000 eV) particles, for example, recoiled Ar and negatively charged oxygen ions, films inevitably contain defects that can act as recombination centres. However, if the deposition is done under HWP, defects can be reduced via low energy particles arising from scattering of process gas (thermalization). Indeed, a better photocatalytic effect was also observed under HWP in TiO_2.[40] Therefore, we can expect the possible existence of recombination centres deteriorating the performance in conventionally sputtered ZnO films and higher quality from HWP-sputtered ZnO, which will improve mobility of electrons and electron-collecting efficiency at the interface between ZnO and the active layer.[41]

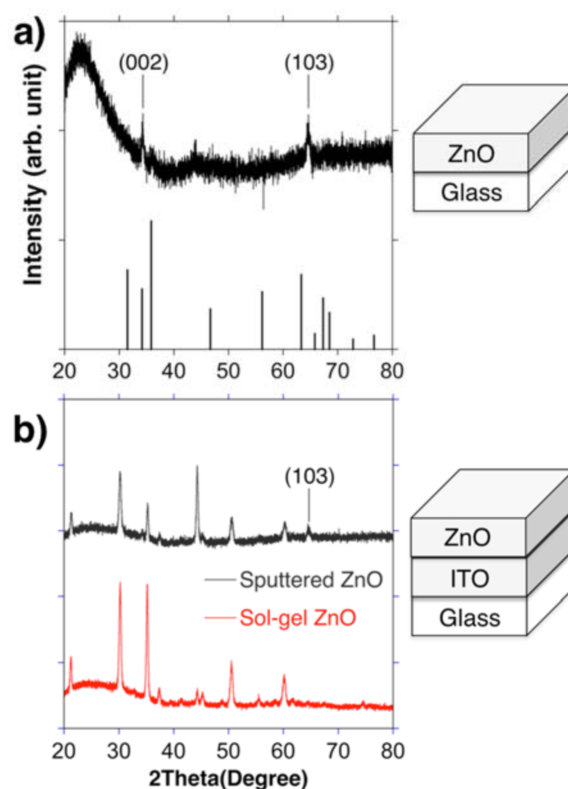

Fig. 2. XRD data of (a) HWP-sputtered ZnO film on glass (JCPDS card No 36-1451 for ZnO), and (b) HWP-sputtered ZnO (black) and sol-gel ZnO (red) each on ITO substrates.

We tested the extent to which ZnO thickness, sputter working-pressure, and oxygen partial pressure affect the performance of ZnO in inverted OSCs. We found that the working-pressure of 4.2 Pa and a thickness of 5 nm gave the best performance (Table S1). The PCEs increased with an increase in working-pressure, but too much pressure did not yield working solar cells. Figure S1 shows atomic force microscopy (AFM) images and roughness averages (R_a) of ZnO produced under different working-pressures. R_a marginally increased with increased working-pressure. An increase in sputtering pressure giving a rougher film is well-known.[42] Yet, ZnO film produced under 7.7 × 10 Pa showed extremely high R_a with many islands. We attribute this poor morphology to the poor device performance. To investigate further, we used XRD and XPS. XRD data showed no significant difference among the ZnO films produced under HWP, but the ZnO film

This journal is © The Royal Society of Chemistry 20xx

Please do not adjust margins

produced under a low working-pressure (2.6×10^{-1} Pa) showed a relatively weaker (002) peak at 34.26°, which could be indicative of lower crystallinity of the film (Figure S2). On the other hand, XPS data displayed clearer difference between the pressures (**Figure 3**). Figure 3a shows Zn $2p_{3/2}$ peaks in which lower binding energy implies that more Zn atoms are bound to O atoms.[43] Also, Figure 3b shows O 1s peaks in which the peak with lower binding energy corresponds to O atoms in a ZnO matrix and the peak with higher binding energy corresponds to oxygen-deficient species which are defects.[45,46] Therefore, the ZnO film fabricated under HWP (4.2 Pa) shows the maximum Zn-O bonds in ZnO matrix and the minimum O defects. This is one of the underlying causes of the high performance of the HWP-sputtered ZnO-based OSCs.

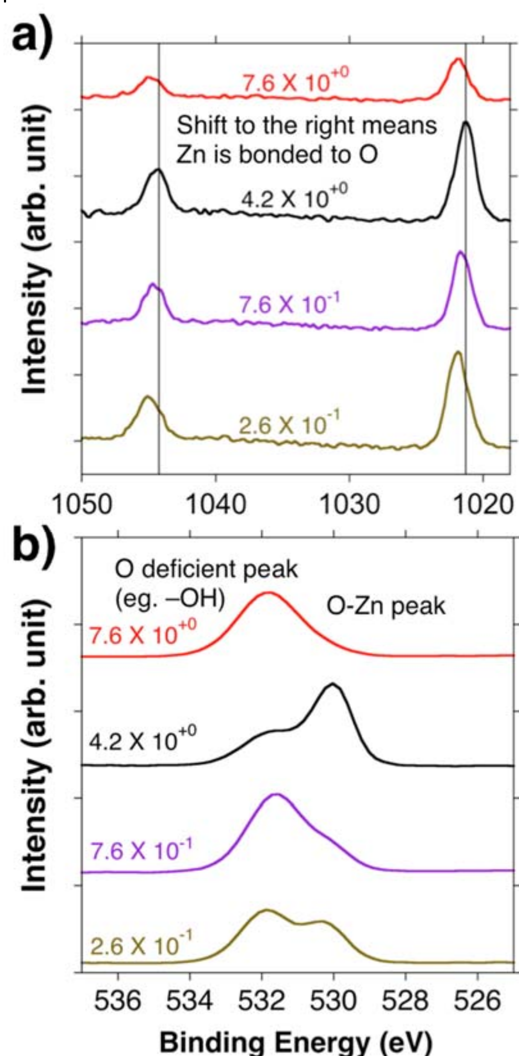

Fig. 3. XPS spectra corresponding to (a) Zn $2p_{3/2}$ and (b) O 1s of HWP-sputtered ZnO films under different working-pressures.

The partial pressure of oxygen during the sputter process affects the quality of ZnO films.[46] In order to find out its effect on HWP-sputtered ZnO, partial pressure of oxygen was varied from 0% to 7%. Table S2 shows PCEs of inverted OSCs fabricated using sputtered ZnO film under 0% to 7% oxygen partial pressures. Reading the table and the *J*–*V* curves in Figure S3, we can observe that all photovoltaic parameters drop with the increase in the partial pressure and 1% partial pressure displays the optimal performance. A partial pressure of 0% oxygen did not yield a working solar cell, indicating that it is crucial to have oxygen during sputtering to ensure the ratio of Zn:O is 1:1. While AFM images show no morphological difference among the samples (Figure S4), XRD spectra show ZnO sputtered under 1% partial pressure possessing a strong (002) peak (Figure S5). The XPS data more clearly displays the quality of the ZnO film by revealing the strongest O-Zn peak and weakest O defect peak for the ZnO sputtered under 1% partial pressure (Figure S6).

Data obtained in previous studies[36,47] indicate that using high temperature annealing on sputtered ZnO improves the performance of OSCs by inducing structural changes of the ZnO surface. According to Jouane *et al.*,[36] sputtered ZnO films annealed at high temperatures demonstrated improvement in performance when used in OSCs. In our study, HWP-ZnO (4.2 Pa) films were annealed at different temperatures from 200 °C to 400 °C in air and in N_2. Table S3 shows the photovoltaic performance recorded. The thermal annealing decreases the performance of the OSC devices substantially. Although both annealing in air and N_2 decreased the PCEs, annealing in N_2 significantly decreased the performance over the increase in annealing temperature. Figure S7 shows the results obtained using AFM. While there is no apparent change for the ZnO samples annealed in air, thermal annealing in N_2 created severe aggregations with the increase in annealing temperatures. From the XPS data, it is clear that thermal annealing ZnO in air increases the O deficient peak at 532 eV, at the same time O-Zn peak at 530 eV decreases with annealing (Figure S8). The position of the Zn $2p_{3/2}$ peaks also corroborates with the peaks from annealed ZnO films, which have higher binding energy than that of non-annealed ZnO. The same was true for the ZnO films annealed in N_2, except the O-Zn peak disappeared and strong O deficient peaks appeared immediately after they were annealed (Figure S9). This is because they were annealed under no oxygen. Based on these results, we conclude that thermal annealing does not improve HWP-ZnO film in OSCs.

Through various optimizations, we have found the optimum working-pressure to be 4.2 Pa, thickness to be under 20 nm, and oxygen partial pressure to be 1% without thermal annealing. Inverted OSCs using P3HT:PC_{61}BM and PTB7:PC_{71}BM were fabricated using the optimized HWP-sputtered ZnO. The best data out of 10 cells from each condition are demonstrated in Table 1. The *J*–*V* curves are displayed in **Figure 4**. For both the P3HT and PTB7 systems, PCEs were substantially increased. This increase resulted mainly from the fill factor (FF), which was determined by low series resistance (R_S). This is surmised to be due to reduced recombination

centers from HWP sputtering. HWP-sputtered ZnO-based devices showed higher open-circuit voltage (V_{OC}) compared to the sol-gel ZnO-based devices, as can be seen from the PTB7-based devices. Although such an increase in V_{OC} was also observed from the P3HT system, the difference was more

frequently observed from the PTB7 system due to intrinsically high V_{OC} value. The difference in the short-circuit current density (J_{SC}) values were subtle. The concurrent increase or decrease in J_{SC} was sample dependent. Although, HWP-sputtered ZnO showed slightly higher transmittance especially below the wavelengths of 400 nm than sol-gel ZnO (Figure S10), our conjecture is that it is not sufficient for an optical effect to take place. The recorded PCE of HWP-sputtered ZnO-based P3HT:PCBM OSCs is the highest reported in literature to our knowledge (Figure S11), and the PCE of the PTB7:$PC_{71}BM$ OSC is also high among the reported values.

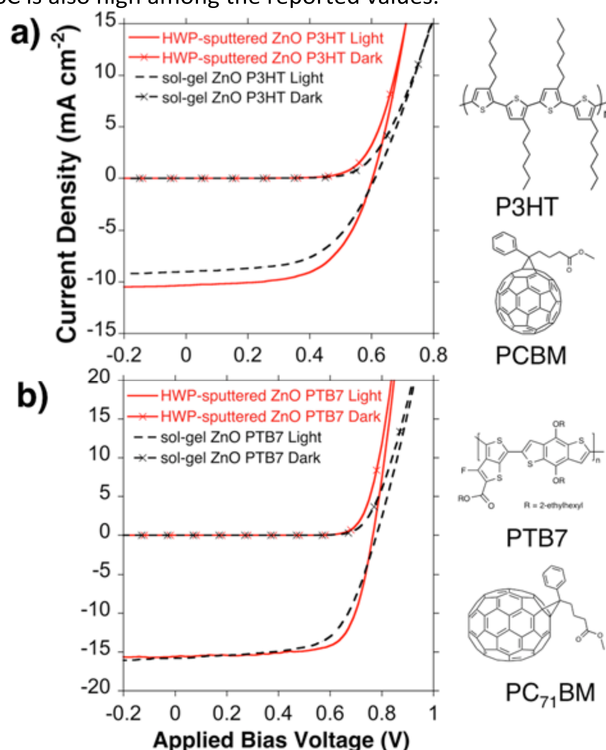

Fig. 4. *J–V* curves of the sol-gel ZnO-based devices and HWP-sputtered ZnO-based devices in (a) P3HT and (b) PTB7 system under 1 sun and in dark.

It is necessary to address previous works in which sputtering was used to grow ZnO films and OSCs were fabricated. Figure S4 shows the reported PCEs from literature and working-pressure used during sputtering. We can observe that a positive correlation between the PCEs and working-pressure used. However, there were some exceptions: for example, Jouane et al. reached almost 3% at low working-pressure, but high temperature (500°C) annealing of ZnO was involved.[36] Zhu et al.[33,37] reported around 3.6%, but they had to undergo two-step sputtering. Furthermore, no standard reference device was demonstrated while J_{SC} was well over 12 mA cm^{-2}, which is unusual for a P3HT:PCBM device. Therefore, it cannot be deemed as valid a comparison.[48]

Implementing the demonstrated technique, flexible inverted OSCs were fabricated on a PET/ITO substrate. While high performance sol-gel ZnO requires annealing temperature above the glass transition temperature (T_g) of PET, HWP-sputtered ZnO is a room temperature process. **Figure 5** shows photovoltaic data and *J-V* curves of the flexible inverted OSC with a picture as an inset. FF was low due to intrinsic high sheet resistance of the PET/ITO. Also we suspect chlorobenzene, the solvent used to dissolve PTB7:$PC_{71}BM$ might have damaged the substrate. Nevertheless, a decent PCE of 4.4% was achieved.

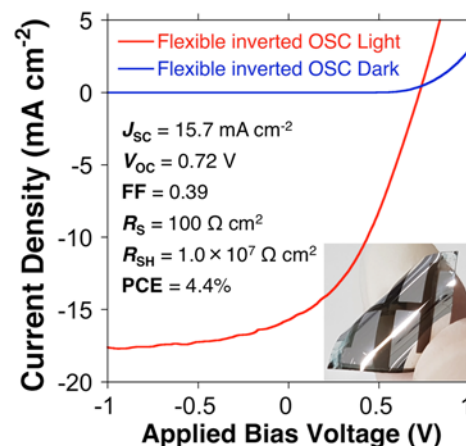

Fig. 5. *J–V* curves of flexible inverted OSC made by sputtered ZnO on ITO PET, with corresponding photovoltaic parameters, and a picture as an inset.

Conclusions

In summary, we have presented the effectiveness of HWP-sputtering technique in producing room temperature and high quality ZnO film for inverted OSCs. Moreover, its flexible application was demonstrated. As noted earlier, XPS served as the most informative when it comes to analyzing the sputtered ZnO films. Strong O-Zn peak and weak O deficient peak of optimized HWP-sputtered ZnO evidenced high quality. Also, the crystallinity of the c-axis (002) peak was strong from XRD, indicating improvement in electron mobility, which was reflected by lowering R_S. Our results provide compelling evidence for the excellence of sputtering technique over the conventional sol-gel process. Future work should therefore include its follow-up applications in various other

Table 1. Photovoltaic data of solar cell devices with sol-gel ZnO as the reference, conventionally sputtered ZnO, and HWP-sputtered ZnO under 1 sun (AM1.5G illumination, 100 mW cm^{-2}).

ETL	Active Layer	V_{OC} (V)	J_{SC} (mA cm^{-2})	FF	R_S (Ω)	R_{SH} (Ω)	PCE (%)
sol-gel ZnO	P3HT:PCBM	0.61	9.08	0.56	17	1.1×10^4	3.07
HWP-sputtered ZnO		0.61	10.3	0.60	3	7.9×10^3	3.71
sol-gel ZnO	PTB7:$PC_{71}BM$	0.73	16.0	0.65	7	$5.7\text{x}10^6$	7.81
HWP-sputtered ZnO		0.77	15.6	0.72	3	$2.7\text{x}10^6$	8.58

This journal is © The Royal Society of Chemistry 20xx

Please do not adjust margins

Please do not adjust margins

photovoltaics such as perovskite solar cells to evaluate their effectiveness when other aspects are concerned. Table 1. Photovoltaic data of solar cell devices with sol-gel ZnO as the reference, conventionally sputtered ZnO, and HWP-sputtered ZnO under 1 sun (AM1.5G illumination, 100 mW cm^{-2}).

Notes and references

Acknowledgements

This work was supported by a Grant-in-Aid for Scientific Research (15H05760 and 16H04187) and the CREST project. I.J. thanks the Japan Society for the Promotion of Science for financial support.

References

1 B. C. Thompson and J. M. J. Fréchet, *Angew. Chemie Int. Ed.*, 2008, **47**, 58–77.
2 J. Nelson, *Mater. Today*, 2011, **14**, 462–470.
3 G. Dennler, M. C. Scharber and C. J. Brabec, *Adv. Mater.*, 2009, **21**, 1323–1338.
4 D. Angmo and F. C. Krebs, *J. Appl. Polym. Sci.*, 2013, **129**, 1–14.
5 K.-S. Chen, H.-L. Yip, J.-F. Salinas, Y.-X. Xu, C.-C. Chueh and A. K.-Y. Jen, *Adv. Mater.*, 2014, **26**, 3349–3354.
6 I. Jeon, K. Cui, T. Chiba, A. Anisimov, A. G. Nasibulin, E. I. Kauppinen, S. Maruyama and Y. Matsuo, *J. Am. Chem. Soc.*, 2015, **137**, 7982–7985.
7 M. Kaltenbrunner, M. S. White, E. D. Głowacki, T. Sekitani, T. Someya, N. S. Sariciftci and S. Bauer, *Nat. Commun.*, 2012, **3**, 770.
8 P. P. Boix, J. Ajuria, I. Etxebarria, R. Pacios, G. Garcia-Belmonte and J. Bisquert, *J. Phys. Chem. Lett.*, 2011, **2**, 407–411.
9 J. You, C.-C. Chen, L. Dou, S. Murase, H.-S. Duan, S. A. Hawks, T. Xu, H. J. Son, L. Yu, G. Li and Y. Yang, *Adv. Mater.*, 2012, **24**, 5267–5272.
10 C. E. Small, S. Chen, J. Subbiah, C. M. Amb, S.-W. Tsang, T.-H. Lai, J. R. Reynolds and F. So, *Nat. Photonics*, 2011, **6**, 115–120.
11 A. Roy, S. H. Park, S. Cowan, M. H. Tong, S. Cho, K. Lee and A. J. Heeger, *Appl. Phys. Lett.*, 2009, **95**, 013302.
12 A. Gadisa, Y. Liu, E. T. Samulski and R. Lopez, *ACS Appl. Mater. Interfaces*, 2012, **4**, 3846–3851.
13 A. K. Kyaw, D. H. Wang, V. Gupta, J. Zhang, S. Chand, G. C. Bazan and A. J. Heeger, *Adv. Mater.*, 2013, **25**, 2397–2402.
14 E. A. Meulenkamp, *J. Phys. Chem. B*, 1998, **102**, 5566–5572.
15 F. C. Krebs, *Sol. Energy Mater. Sol. Cells*, 2009, **93**, 394–412.
16 S. K. Hau, H.-L. Yip, N. S. Baek, J. Zou, K. O'Malley and A. K.-Y. Jen, *Appl. Phys. Lett.*, 2008, **92**, 253301.
17 S. K. Hau, H.-L. Yip, H. Ma and A. K.-Y. Jen, *Appl. Phys. Lett.*, 2008, **93**, 233304.
18 T. Kuwabara, T. Nakashima, T. Yamaguchi, K. Takahashi, *Org. Electron.* 2012, **13**, 1136-1140.
19 T. Kuwabara, X. Wang, T. Kusumi, T. Yamaguchi, T. Taima, K. Takahashi, *Jpn. J. Appl. Phys.* 2016, **55**, 086501.
20 I. Jeon, J. W. Ryan, T. Nakazaki, K. S. Yeo, Y. Negishi and Y. Matsuo, *J. Mater. Chem. A*, 2014, **2**, 18754–18760.
21 K.-S. Shin, H.-J. Park, B. Kumar, K.-K. Kim, S.-G. Ihn and S.-W. Kim, *J. Mater. Chem.*, 2011, **21**, 12274.
22 S. Alem, J. Lu, R. Movileanu, T. Kololuoma, A. Dadvand and Y. Tao, *Org. Electron.*, 2014, **15**, 1035–1042.
23 J. Hu, Z. Wu, H. Wei, T. Song and B. Sun, *Org. Electron.*, 2012, **13**, 1171–1177.
24 C. Zhang, H. You, Z. Lin and Y. Hao, *Jpn. J. Appl. Phys.*, 2011, **50**, 082302.
25 Y. Sun, J. H. Seo, C. J. Takacs, J. Seifter and A. J. Heeger, *Adv. Mater.*, 2011, **23**, 1679–1683.
26 M. D. Barankin, E. Gonzalez II, A. M. Ladwig and R. F. Hicks, *Sol. Energy Mater. Sol. Cells*, 2007, **91**, 924–930.
27 H. Cheun, C. Fuentes-Hernandez, Y. Zhou, W. J. Potscavage, S.-J. Kim, J. Shim, A. Dindar and B. Kippelen, *J. Phys. Chem. C*, 2010, **114**, 20713–20718.
28 C. Klingshirn, *Phys. status solidi*, 2007, **244**, 3027–3073.
29 Y. Jouane, S. Colis, G. Schmerber, P. Kern, A. Dinia, T. Heiser and Y.-A. Chapuis, *J. Mater. Chem.*, 2011, **21**, 1953–1958.
30 28 Y.-S. Park, K.-H. Choi and H.-K. Kim, *J. Phys. D. Appl. Phys.*, 2009, **42**, 235109.
31 29 W. Shin, T. Yasuda, G. Watanabe, Y. S. Yang and C. Adachi, *Chem. Mater.*, 2013, **25**, 2549–2556.
32 30 F. Zhu, X. Chen, J. Zhou, Z. Lu, Y. Chen, S. Huang and Z. Sun, *Mater. Res. Express*, 2014, **1**, 25020.
33 31 Y. Jouane, S. Colis, G. Schmerber, A. Dinia, P. Lévêque, T. Heiser and Y. Chapuis, *Org. Electron.*, 2013, **14**, 1861–1868.
34 32 J. Lee, B. Hong and Y. S. Park, *Thin Solid Films*, 2013, **547**, 3–8.
35 33 Y. Jouane, S. Colis, G. Schmerber, A. Dinia, P. Bazylewski, G. S. Chang and Y. Chapuis, *Thin Solid Films*, 2015, **576**, 23–30.
36 34 F. Zhu, X. Chen, L. Zhou, J. Zhou, J. Yang, S. Huang and Z. Sun, *Thin Solid Films*, 2014, **551**, 131–135.
37 35 S. Flickyngerova, K. Shtereva, V. Stenova, D. Hasko, I. Novotny, V.Tvarozek, P. Sutta and E. Vavrinsky, *Appl. Surf. Sci.*, 2008, **254**, 3643–3647.
38 36 J. A. Thornton, *J. Vac. Sci. Technol.*, 1974, **11**, 666.
39 37 M. Yamagishi, S. Kuriki, P. K. Song and Y. Shigesato, *Thin Solid Films*, 2003, **442**, 227–231.
40 38 N. Sekine, C.-H. Chou, W. L. Kwan and Y. Yang, *Org. Electron.*, 2009, **10**, 1473–1477.
41 39 K. Srinivas, M. Manivel Raja, D. V. Sridhara Rao and S. V. Kamat, *Thin Solid Films*, 2014, **558**, 349–355.
42 40 M. Chen, X. Wang, Y. . Yu, Z. . Pei, X. . Bai, C. Sun, R. . Huang and L. . Wen, *Appl. Surf. Sci.*, 2000, **158**, 134–140.
43 41 Y. Zhang, G. Du, X. Wang, W. Li, X. Yang, Y. Ma, B. Zhao, H. Yang, D. Liu and S. Yang, *J. Cryst. Growth*, 2003, **252**, 180–183.
44 42 X. Q. Wei, B. Y. Man, M. Liu, C. S. Xue, H. Z. Zhuang and C. Yang, *Phys. B Condens. Matter*, 2007, **388**, 145–152.
45 43 P. F. Carcia, R. S. McLean, M. H. Reilly and G. Nunes, *Appl. Phys. Lett.*, 2003, **82**, 1117.
46 44 Y. I. Alivov, X. Bo, S. Akarca-Biyikli, Q. Fan, J. Xie, N. Biyikli, K. Zhu, D. Johnstone and H. Morkoç, *J. Electron. Mater.*, 2006, **35**, 520–524.
47 45 Y.-H. Hu, Y.-C. Chen, H.-J. Xu, H. Gao, W.-H. Jiang, F. Hu and Y.-X. Wang, *Engineering*, 2010, **2**, 973–978.
48 46 H. J. Snaith, *Nat. Photonics*, 2012, **6**, 337–340.
49 47 Y. Santo, I. Jeon, K. Sheng Yeo, T. Nakagawa and Y. Matsuo, *Appl. Phys. Lett.*, 2013, **103**, 073306.

This journal is © The Royal Society of Chemistry 20xx

Please do not adjust margins